Electronic Supplementary Information

Phase transition in the extreme: a cubic-to-triclinic symmetry change in dielectrically switchable cyanide perovskites

Monika Trzebiatowska[a]*, Anna Gągor[a], Lucyna Macalik[a], Paulina Peksa[b], Adam Sieradzki[b]

[a]*Institute of Low Temperature and Structure Research, Polish Academy of Sciences, Box 1410, 50-950 Wrocław 2, Poland*

[b]*Faculty of Fundamental Problems of Technology, Wrocław University of Technology, Wybrzeże Wyspiańskiego 27, 50-370, Wrocław, Poland*

**corresponding author; e-mail: m.trzebiatowska@intibs.pl*

Table S1. The selected geometric parameters of $FA_2KM(CN)_6$, where M=Co, Fe (Å, °).

$FA_2KCo(CN)_6$ 330 K			
Co1—C3 x 6	1.874 (4)	K2—N1 x 6	2.794 (4)
C—Co—C_{trans}	180.0	N—K—N	180.0
C—Co—C_{cis}	90.000 (1)	N—K—N	90.0
$FA_2KCo(CN)_6$ 290 K			
Co1—C6	1.898 (2)	K2—N5^{v}	2.832 (2)
Co1—C6^{i}	1.898 (2)	K2—N3^{vii}	2.847 (2)
Co1—C8^{i}	1.899 (2)	K2—N3^{vi}	2.847 (2)
Co1—C8	1.899 (2)	N7—C8	1.145 (3)
Co1—C4	1.896 (2)	N9—C11	1.277 (4)
Co1—C4^{i}	1.896 (2)	N3—C6	1.148 (3)
K2—N7^{ii}	2.831 (2)	C4—N5	1.143 (3)
K2—N7^{iii}	2.831 (2)	N10—C11	1.274 (4)
K2—N5^{iv}	2.832 (2)		
C6—Co1—C6^{i}	180.00 (10)	N7^{iii}—K2—N5^{v}	79.16 (8)
C6—Co1—C8^{i}	89.85 (10)	N5^{iv}—K2—N5^{v}	180.0
C6^{i}—Co1—C8^{i}	90.15 (10)	N7^{ii}—K2—N3^{vi}	90.55 (7)
C6—Co1—C8	90.15 (10)	N7^{iii}—K2—N3^{vi}	89.45 (7)
C6^{i}—Co1—C8	89.85 (10)	N5^{iv}—K2—N3^{vi}	87.62 (8)
C8^{i}—Co1—C8	180.0	N5^{v}—K2—N3^{vi}	92.38 (8)
C6—Co1—C4	91.14 (11)	N7^{ii}—K2—N3^{vii}	89.45 (7)
C6^{i}—Co1—C4	88.86 (11)	N7^{iii}—K2—N3^{vii}	90.55 (7)
C8^{i}—Co1—C4	90.72 (10)	N5^{iv}—K2—N3^{vii}	92.38 (8)
C8—Co1—C4	89.28 (10)	N5^{v}—K2—N3^{vii}	87.62 (8)
C6—Co1—C4^{i}	88.86 (11)	N3^{vi}—K2—N3^{vii}	180.00 (17)
C6^{i}—Co1—C4^{i}	91.14 (11)	C6—N3—K2^{viii}	163.3 (2)
C8^{i}—Co1—C4^{i}	89.28 (10)	N5—C4—Co1	176.8 (2)
C8—Co1—C4^{i}	90.72 (10)	C4—N5—K2^{ix}	146.0 (2)

C4—Co1—C4^{i}	180.0	N3—C6—Co1	178.7 (2)
N7^{ii}—K2—N7^{iii}	180.00 (17)	C8—N7—K2^{x}	160.7 (2)
N7^{ii}—K2—N5^{iv}	79.16 (8)	N7—C8—Co1	177.9 (2)
N7^{iii}—K2—N5^{iv}	100.84 (8)	N10—C11—N9	124.6 (3)
N7^{ii}—K2—N5^{v}	100.84 (8)		

$FA_2KFe(CN)_6$ 330 K

Fe1—C3	1.917 (5) x 6	K2—N1^{xv}	2.783 (5) x6
C—Fe—C	90.0	N—K—N	90.0
C—Fe—C^{i}	180.0	N—K—N	180.0

$FA_2KFe(CN)_6$ 290 K

Fe1—C4	1.938 (2)	K2—N7^{iii}	2.8298 (18)
Fe1—C4^{i}	1.938 (2)	K2—N3^{vii}	2.8441 (17)
Fe1—C8	1.938 (2)	K2—N3^{vi}	2.8441 (17)
Fe1—C8^{i}	1.938 (2)	N3—C6	1.143 (2)
Fe1—C6	1.9425 (19)	C4—N5	1.144 (3)
Fe1—C6^{i}	1.9425 (19)	N7—C8	1.147 (2)
K2—N5^{iv}	2.824 (2)	N9—C11	1.269 (3)
K2—N5^{v}	2.824 (2)	N10—C11	1.279 (3)
K2—N7^{ii}	2.8298 (18)		
C4—Fe1—C4^{i}	180.0	N5^{v}—K2—N7^{iii}	79.96 (6)
C4—Fe1—C8	88.75 (8)	N7^{ii}—K2—N7^{iii}	180.00 (7)
C4^{i}—Fe1—C8	91.25 (8)	N5^{iv}—K2—N3^{vii}	92.61 (6)
C4—Fe1—C8^{i}	91.25 (8)	N5^{v}—K2—N3^{vii}	87.39 (6)
C4^{i}—Fe1—C8^{i}	88.75 (8)	N7^{ii}—K2—N3^{vii}	89.71 (5)
C8—Fe1—C8^{i}	180.0	N7^{iii}—K2—N3^{vii}	90.29 (5)
C4—Fe1—C6	92.05 (8)	N5^{iv}—K2—N3^{vi}	87.39 (6)
C4^{i}—Fe1—C6	87.95 (8)	N5^{v}—K2—N3^{vi}	92.61 (6)
C8—Fe1—C6	89.82 (8)	N7^{ii}—K2—N3^{vi}	90.29 (5)
C8^{i}—Fe1—C6	90.18 (8)	N7^{iii}—K2—N3^{vi}	89.71 (5)
C4—Fe1—C6^{i}	87.95 (8)	N3^{vii}—K2—N3^{vi}	180.0
C4^{i}—Fe1—C6^{i}	92.05 (8)	C6—N3—K2^{viii}	161.73 (19)
C8—Fe1—C6^{i}	90.18 (8)	N5—C4—Fe1	177.03 (19)
C8^{i}—Fe1—C6^{i}	89.82 (8)	C4—N5—K2^{ix}	145.63 (18)
C6—Fe1—C6^{i}	180.0	N3—C6—Fe1	178.83 (19)
N5^{iv}—K2—N5^{v}	180.00 (13)	C8—N7—K2^{x}	160.71 (18)
N5^{iv}—K2—N7^{ii}	79.96 (6)	N7—C8—Fe1	177.97 (19)
N5^{v}—K2—N7^{ii}	100.04 (6)	N9—C11—N10	125.0 (3)
N5^{iv}—K2—N7^{iii}	100.04 (6)		

Symmetry codes: (i) -*x*+1, -*y*+1, -*z*+1; (ii) -*x*, -*y*+1, -*z*; (iii) *x*, *y*-1, *z*; (iv) -*x*+1, -*y*+1, -*z*; (v) *x*-1, *y*-1, *z*; (vi) *x*, *y*-1, *z*-1; (vii) -*x*, -*y*+1, -*z*+1; (viii) *x*, *y*+1, *z*+1; (ix) *x*+1, *y*+1, *z*; (x) *x*, *y*+1, *z*; (xi) -*y*+1/2, -*z*+1, -*x*+1/2; (xii) *y*-1/2, *z*, *x*+1/2; (xiii) *z*-1/2, *x*+1/2, *y*; (xiv) -*z*+1/2, -*x*+1/2, -*y*+1; (xv) -*y*+1, -*z*+1, -*x*+1; (xvi) *z*, *x*, *y*; (xvii) -*z*+1, -*x*+1, -*y*+1; (xviii) *y*, *z*, *x*.

Table S2. The atomic displacements from HT to LT positions calculated in Amplimodes for $FA_2KCo(CN)_6$.

$FA_2KCo(CN)_6$			Atomic Displacements			
WP		**Atom**	**ux**	**uy**	**uz**	**|u|**
1h	(1/2,1/2,1/2)	Co1	0.0000	0.0000	0.0000	0.0000
1a	(0,0,0)	K2	0.0000	0.0000	0.0000	0.0000
2i	(x,y,z)	C6	0.0263	0.0260	-0.0247	0.3037
2i	(x,y,z)	C8	-0.0264	-0.0208	0.0228	0.2749
2i	(x,y,z)	C4	0.0627	-0.0549	0.0128	0.5037
2i	(x,y,z)	N3	0.0390	0.0404	-0.0379	0.4610
2i	(x,y,z)	N7	-0.0484	-0.0336	0.0402	0.4797
2i	(x,y,z)	**N5**	**0.1046**	**-0.0950**	**0.0167**	**0.8396**

ux, uy and uz are given in relative units. |u| is the absolute distance given in Å; Maximum atomic displacement in the distortion, Δ: 0.8396 Å; Total distortion amplitude: 1.7715 Å

Table S3. The atomic displacements from HT to LT positions calculated in Amplimodes for $FA_2KFe(CN)_6$.

$FA_2KFe(CN)_6$			Atomic Displacements			
WP		**Atom**	**ux**	**uy**	**uz**	**|u|**
1h	(1/2,1/2,1/2)	Fe1	0.0000	0.0000	0.0000	0.0000
1a	(0,0,0)	K2	0.0000	0.0000	0.0000	0.0000
2i	(x,y,z)	C6	0.0270	0.0289	-0.0267	0.3264
2i	(x,y,z)	C8	-0.0268	-0.0210	0.0224	0.2802
2i	(x,y,z)	C4	0.0633	-0.0566	0.0085	0.5058
2i	(x,y,z)	N3	0.0405	0.0449	-0.0424	0.4986
2i	(x,y,z)	N7	-0.0483	-0.0337	0.0394	0.4824
2i	(x,y,z)	**N5**	**0.1050**	**-0.0975**	**0.0112**	**0.8457**

ux, uy and uz are given in relative units. |u| is the absolute distance given in Å. Maximum atomic displacement in the distortion, Δ: 0.8457 Å; Total distortion amplitude: 1.8096 Å

Table S4. The factor group analysis for $FA_2KM(CN)_6$ (M=Co, Fe) in the LT and HT phase. The data in the parentheses correspond to the HT phase. Note, that the formamidinium cation in the HT phase is highly disordered and therefore its analysis is not given here. The IR-active modes are marked in red, the Raman-active - in blue, the modes active in **both IR and Raman** spectra are in **black** and the silent ones - in green.

Ion	**Vibration**	**Free ion symmetry**	**Site symmetry**	**Factor group symmetry**
		$C_{\infty v}$	**C_1 (C_{4v})**	**C_i (O_h)**
CN^-	ν	A_1	A (A_1)	A_g+A_u ($2A_{1g}$+$2E_g$)
	T'	A_1+E_1	3A (A_1+E)	$3A_g$+$3A_u$ ($2F_{2g}$+$4F_{1u}$)
	L	A_2+E_1*	2A (A_2+E)*	$2A_g$+$2A_u$ ($2F_{1g}$+$2F_{2u}$)
		C_{2v}	**C_1**	**C_i**
FA^+	$\nu_s NH_2$	A_1+B_1	2A	$2A_g$+$2A_u$
	$\nu_{as} NH_2$	A_1+B_1	2A	$2A_g$+$2A_u$
	δNH_2	A_1+B_1	2A	$2A_g$+$2A_u$
	ρNH_2	A_1+B_1	2A	$2A_g$+$2A_u$
	ωNH_2	A_2+B_2	2A	$2A_g$+$2A_u$
	τNH_2	A_2+B_2	2A	$2A_g$+$2A_u$
	$\nu_s NCN$	A_1	A	A_g+A_u

	ν_{as}NCN	B_1	A	A_g+A_u
	δNCN	A_1	A	A_g+A_u
	νCH	A_1	A	A_g+A_u
	δCH	B_1	A	A_g+A_u
	γCH	B_2	A	A_g+A_u
	T'	A_1+B_1+B_2	3A	3A_g+3A_u
	L	A_2+B_1+B_2	3A	3A_g+3A_u
M^{3+}			**C_i (O_h)**	**C_i (O_h)**
			3A_u (F_{1u})	3A_u (F_{1u})
K^+			**C_i (O_h)**	**C_i (O_h)**
			3A_u (F_{1u})	3A_u (F_{1u})
*one L is subtracted				

Table S5. The observed Raman and IR modes (in cm^{-1}) of $FA_2KM(CN)_6$ (M=Co, Fe) and their proposed assignment.

$FA_2KCo(CN)_6$				**$FA_2KFe(CN)_6$**		**Assignment**
IR		**Raman**		**IR**		
80 K	**350 K**	**80 K**	**350 K**	**80 K**	**350 K**	
3441s	3442s	3437w	3440w	3442s	3444s	$\nu_{as}NH_2$ 2xδNH_2
3423s	3379s			3423s		$\nu_{as}NH_2$
3372s				3372m	3382m	combination
3344s			3345m	3342m		$\nu_{as}NH_2$
3306s		3307m		3306m		$\nu_{as}NH_2$ $\nu_s NH_2$
3291s	3284s	3291w		3291m	3287s	combination
3264s		3264m	3250m	3261s		$\nu_s NH_2$
3236s		3229m		3236s		$\nu_s NH_2$
3188s	3192s			3188m	3193m	combination
3156s				3157m		combination
		3097m	3096w	3121sh		combination
3025sh		3038w	3031w	3025w	3034w	νCH
2834w	2828vw			2835w	2823vw	combination
2785w				2786vw		combination
2755w				2757w	2747w	combination
2739w	2744w			2739w		combination
2705vw				2656vw		combination
2658w	2657vw			2628vw		2xρNH_2
2624w				2586vw		2xρNH_2
2588w				2511vw		2xρNH_2
2551w				2459vw		combination
2544w	2538vw					combination
		2153vs	2148vs	2118s	2114s	νCN
2129vs	2125vs	2138vs	2135s			νCN
1716vs	1722vs			1716vs	1723vs	δNH_2
1625m	1636w	1622vw		1623w	1640vw	δNH_2

1582vw			1568vw			δNH_2
1557w	1556vw	1552vw				$\nu_{as}NCN$
1400m	1397m	1403w	1396m	1401m	1402m	δCH
1342m	1341m	1346vw		1342m	1343m	ρNH_2
1270m	1260m			1268m	1245w	ρNH_2
1219w				1219w		ρNH_2
1125w	1116vw	1123w	1115w	1125w	1111vw	$\nu_s NCN$
1055m	1065w	1055w		1055m	1065w	ωNH_2
1041m	1029vw			1042w		ωNH_2
896w	893vw			876vw	874vw	combination
				828vw	825vw	combination
771w				772w		γCH
				747vw	741vw	combination
668m	667m	654vw	666vw	675m	639m	$\delta NCN\ \tau NH_2$
628s	641s			627m		τNH_2
586m						τNH_2
565m						$T'CN^-$
		532vw	528vw			$T'CN^-$
		415m	411m			$T'CN^-$
		342vw				$T'CN^-$
		331vw				$T'FA^+$
		209w				$LCN^- T'M^{3+}$
		179m				$LCN^- T'M^{3+} T'FA^+$
		140w	147m			$T'M^{3+}$
		114w				$LM^{3+} LFA^+$
		106w				$LM^{3+} LFA^+$

Key: s-very strong, s-strong, m-medium, w-weak, vw-very weak, sh-shoulder; ν_s–symmetric stretching, ν_{as}-asymmetric stretching, δ-in-plane bending (scissoring), ρ-rocking, ω-wagging, τ-twisting (torsion), γ-out-of-plane bending, T–translation, L–libration.

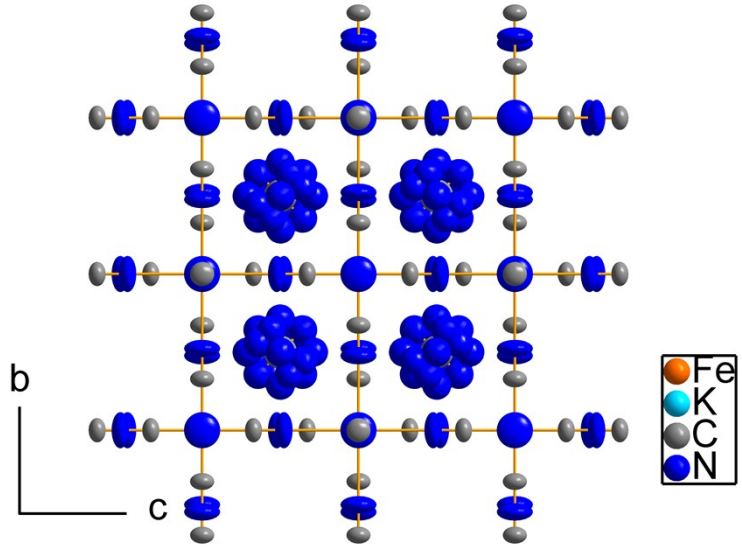

Figure S1. The crystal structure of $FA_2KFe(CN)_6$ at 330 K in the cubic phase. The anisotropic displacement parameters are drawn at 50% probability level.

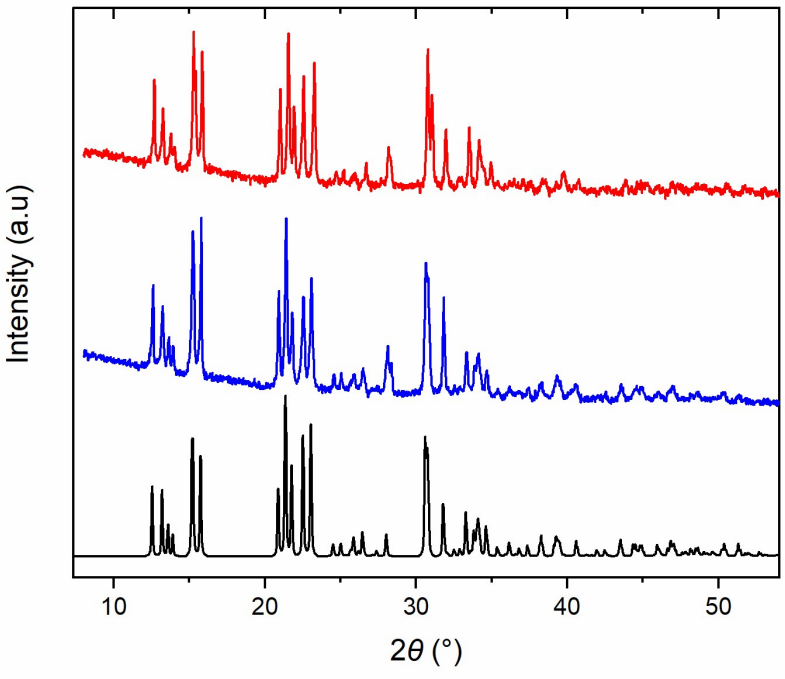

Figure S2. The powder X-ray diffraction patterns: of $FA_2KCo(CN)_6$ (red), $FA_2KFe(CN)_6$ (blue) referred against a **calculated** pattern based on the crystal structure of Co-sample (**black**).

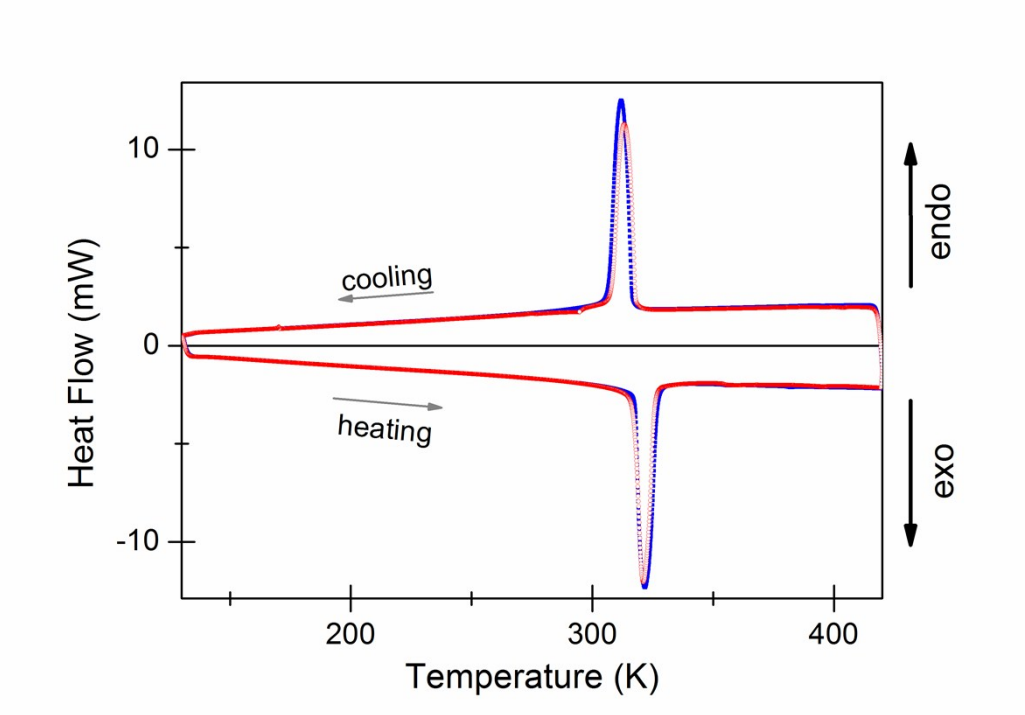

Figure S3. DSC traces for the $FA_2KCo(CN)_6$ (red) and $FA_2KFe(CN)_6$ (blue) samples in heating and cooling modes at constant sweeping rate 5 K/min.

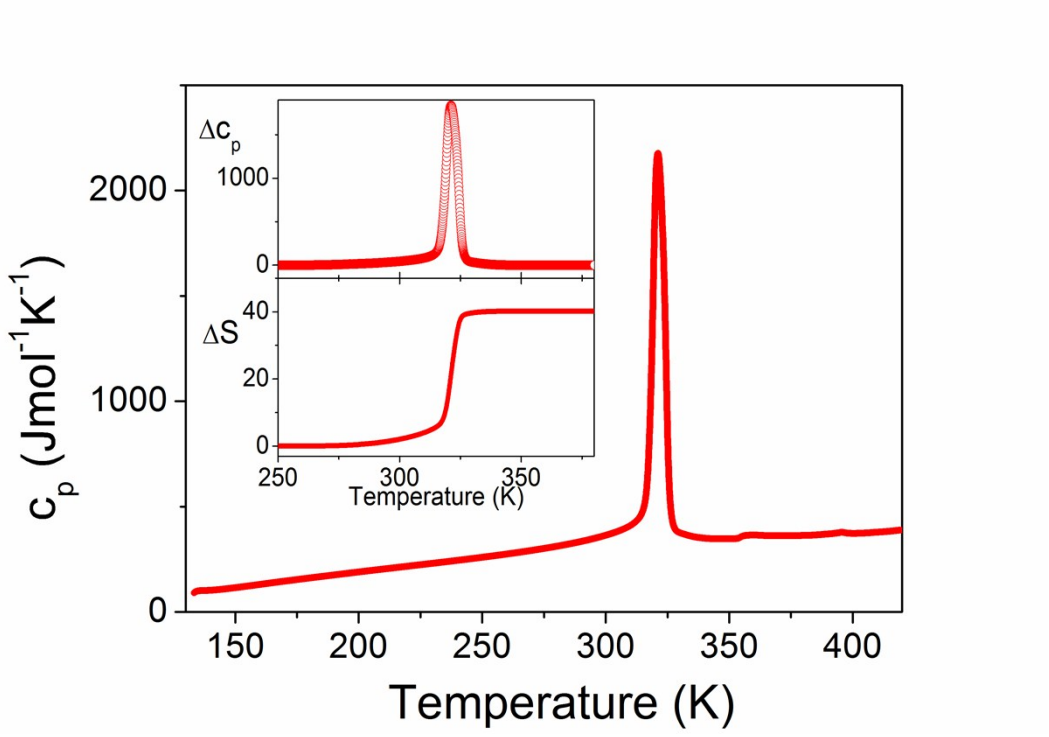

Figure S4. The heat capacity of $FA_2KFe(CN)_6$ measured in a heating mode. The insets show the change in Cp and S related to the phase transition.

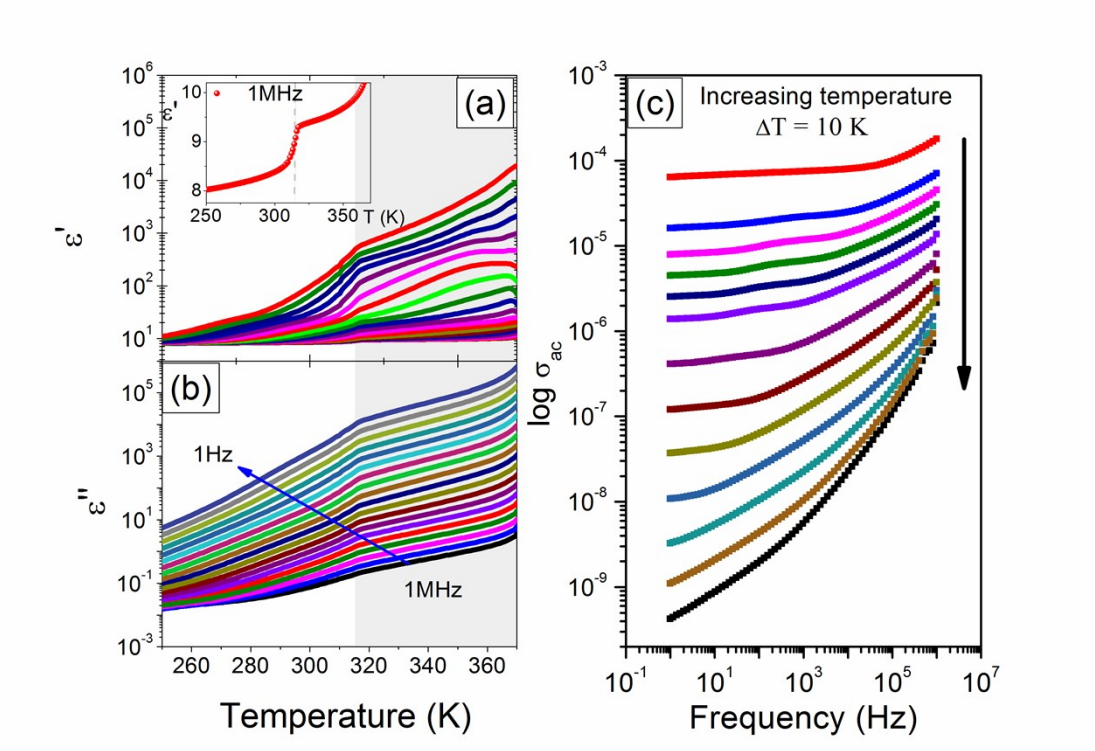

Figure S5. The temperature dependence of real part of dielectric permittivity (a) and dielectric loss (b) and the compilation of the data for the AC conductivity below (c) and above (d) the phase transition temperature of a polycrystalline pellet $FA_2KFe(CN)_6$.

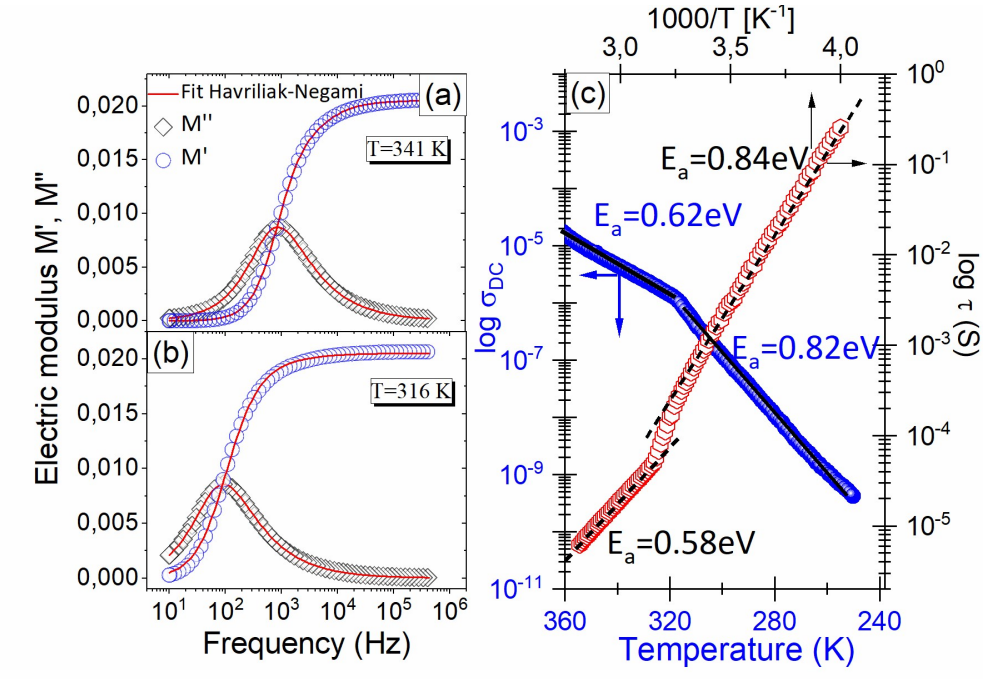

Figure S6. The experimental data fitted according to H-N (a) (b) and a relaxation map as a function of 1000/T (red) and the compilation of the data for the DC conductivity (blue) (c) of polycrystalline pellet $FA_2KFe(CN)_6$.

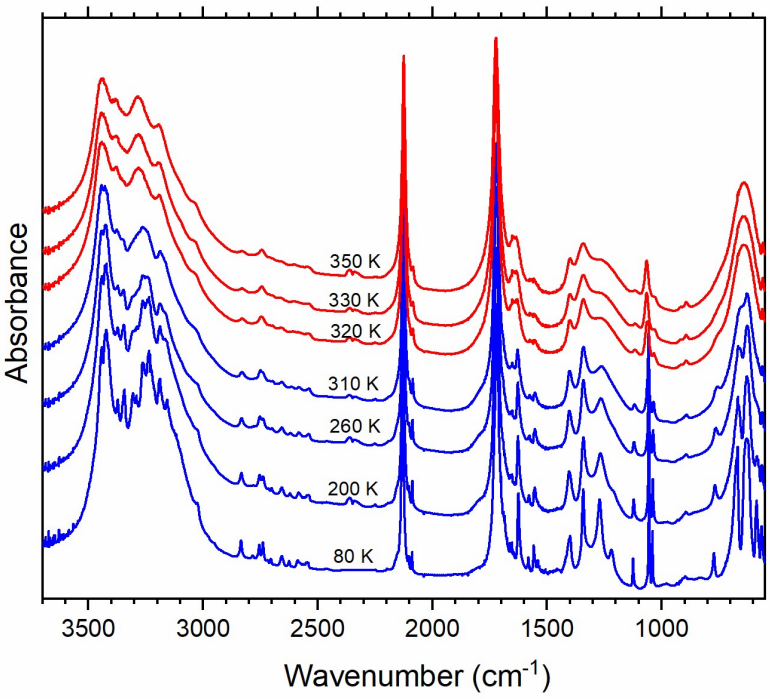

Figure S7. The temperature-dependent IR spectra in the full wavenumber range of $FA_2KCo(CN)_6$.

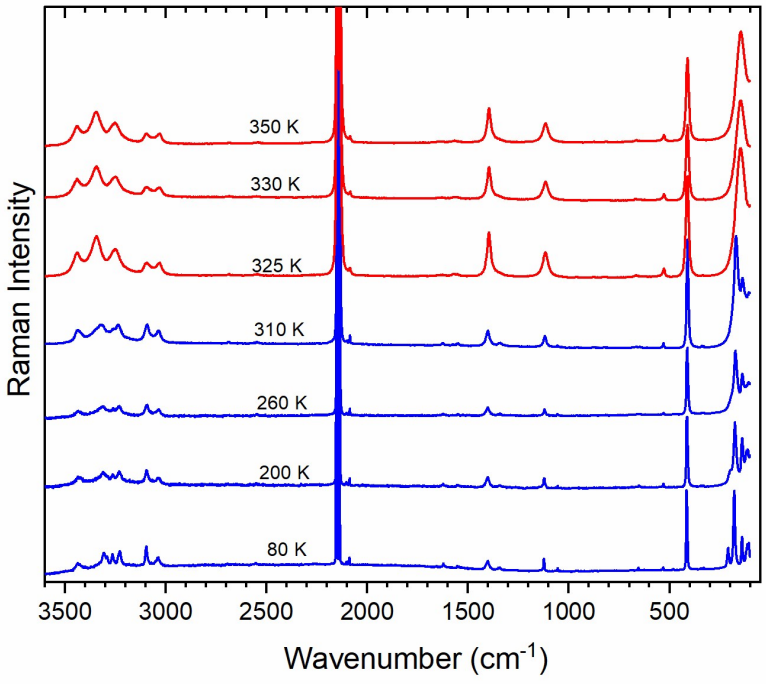

Figure S8. The temperature-dependent Raman spectra in the full wavenumber range of $FA_2KCo(CN)_6$.

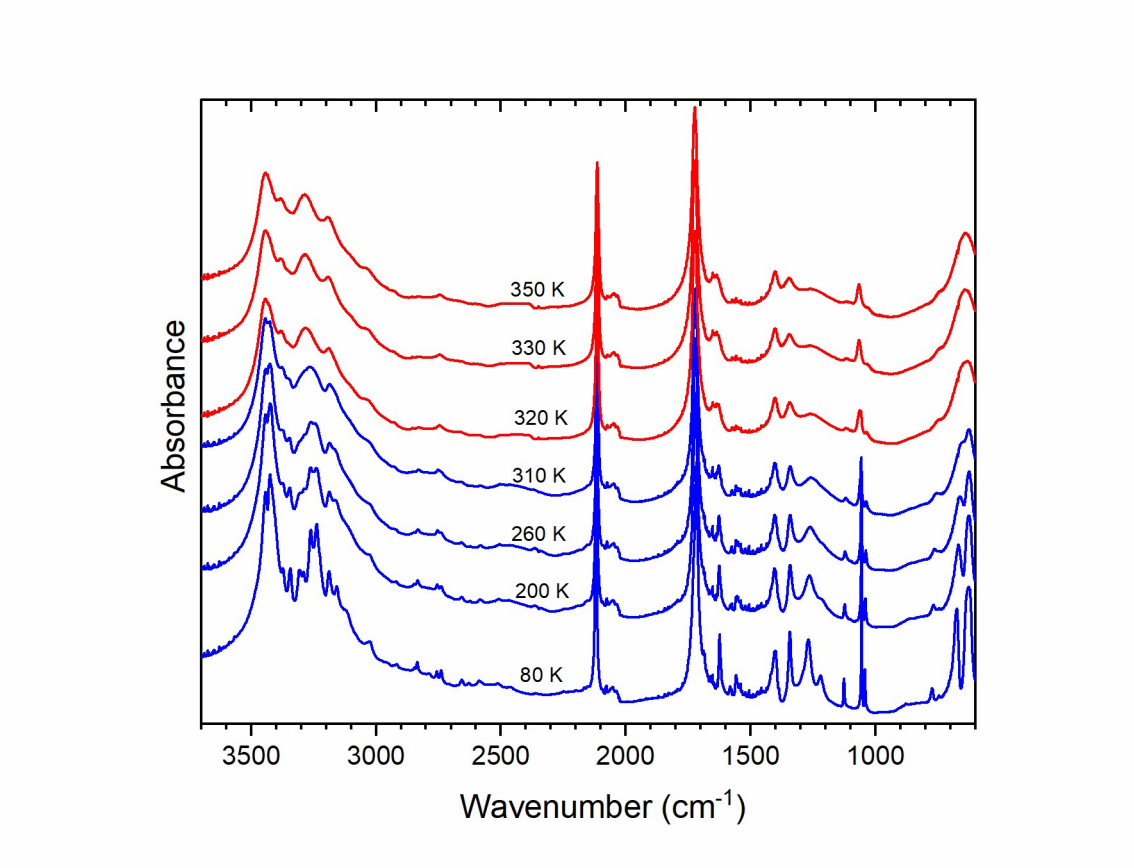

Figure S9. The temperature-dependent IR spectra in the full wavenumber range of $FA_2KFe(CN)_6$.

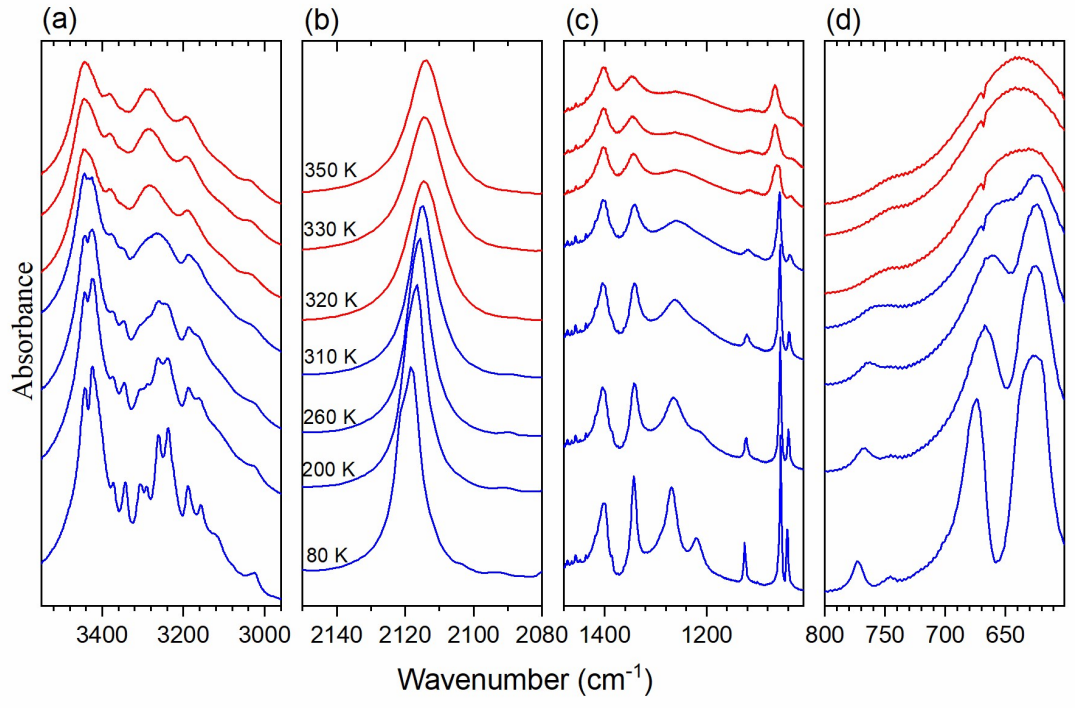

Figure S10. The details of the temperature-dependent IR spectra of $FA_2KFe(CN)_6$.

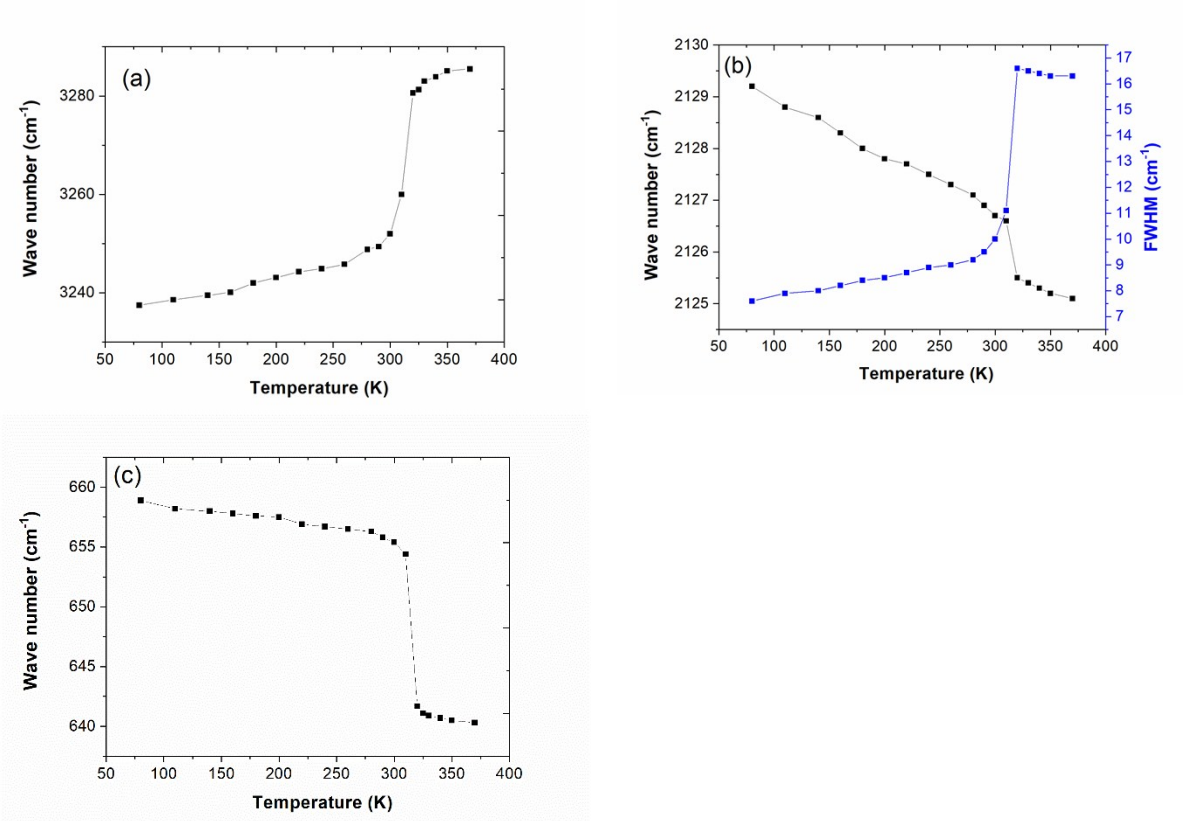

Figure S11. The plots of the wavenumber and FWHM *vs*. T of the selected IR modes: (a) $\nu_{as}NH_2$, (b) νCN^- and (c) τNH_2 in $FA_2KCo(CN)_6$.

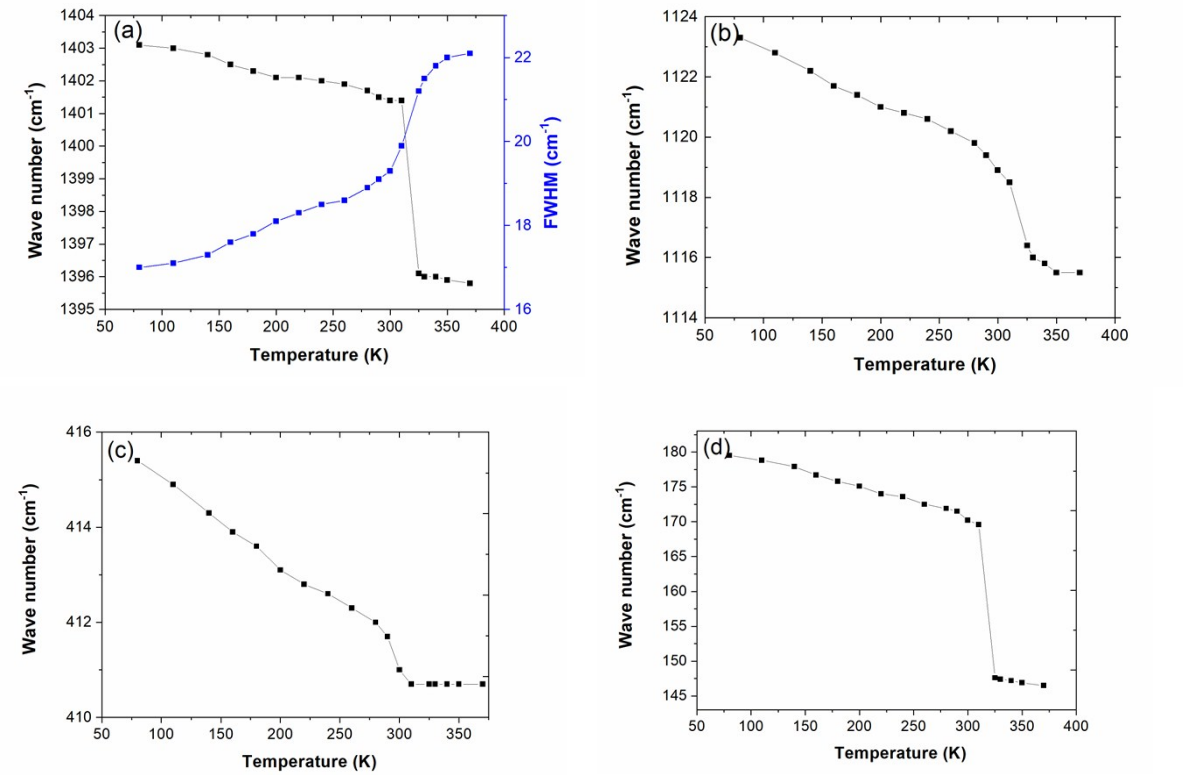

Figure S12. The plots of the wavenumber and FWHM *vs*. T of the selected Raman modes: (a) δCH, (b) $\nu_s NCN$, (c) T'CN and (d) lattice modes in $FA_2KCo(CN)_6$.

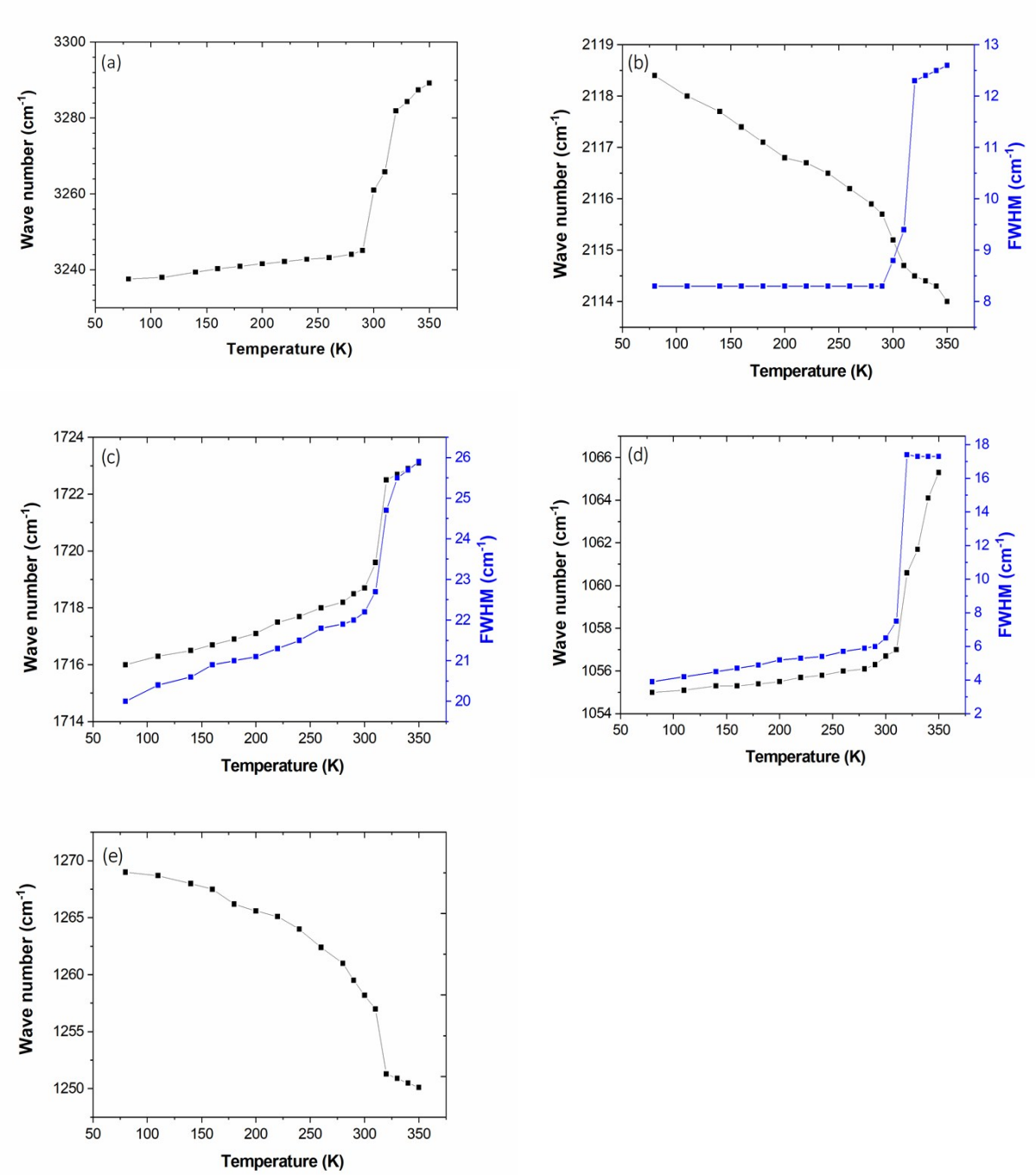

Figure S13. The plots of the wavenumber and FWHM *vs*. T of the selected IR modes: (a) $\nu_{as}NH_2$, (b) νCN^-, (c) δNH_2, (d) ωNH_2 and (e) ρNH_2 in $FA_2KFe(CN)_6$.